Flow Measurement and Instrumentation 96 (2024) 102535

Contents lists available at ScienceDirect

Flow Measurement and Instrumentation

journal homepage: www.elsevier.com/locate/flowmeasinst

Extending the pressure-time method to bend using 3D-CFD

Mehrdad Kalantar Neyestanaki [a,*], Georgiana Dunca [b], Pontus Jonsson [c], Michel J. Cervantes [a]

[a] Department of Engineering Sciences and Mathematics, Luleå University of Technology, Sweden
[b] Department of Hydraulics, Hydraulic Machinery and Environmental Engineering, University Politehnica of Bucharest, Romania
[c] Vattenfall AB, Sweden

ARTICLE INFO

Keywords:
Pressure-time method out of IEC 60041
Low-head hydraulic turbine
Bend
3D CFD

ABSTRACT

According to the IEC 60041 standard, the pressure-time method (1D PTM) can be employed to determine the flow rate in hydraulic turbines. This method assumes a one-dimensional flow and applies to straight pipes with uniform cross-sections, with specific restrictions on the pipe length, fluid velocity, and distance between the measurement sections from any irregularities in the pipeline. However, challenges arise when applying this method in low-head hydropower plants due to the short lengths, irregularities like bends and developing flows in the intake. The present paper aims to improve the performance of the method in the presence of a bend. To this end, a test rig has been developed and measurements performed, including such geometry.

The data are evaluated using the development of a newly proposed approach combining the 1D PTM based on an energy balance formulation and three-dimensional computational fluid dynamics (3D CFD) developed for axis-symmetrical accelerating flows. The updated methodology includes a correction of the experimental pressure measurements used in the 1D PTM to account for the effects of the Dean vortices present after the bend as well as the kinetic energy correction factors which deviate from known values in transient conditions.

The results obtained under conditions involving the presence of bends either between or in close proximity to one show a significant improvement compared to the standard one-dimensional pressure-time method.

1. Introduction

Hydropower was ranked as the third-largest energy source worldwide, accounting for 17 % of global electricity production in 2019 [1]. Many hydropower plants were built many years ago; therefore, their refurbishment is required to preserve their operation and even improve them. It is important to assess the efficiency of renovated turbines before and after refurbishment to meet performance guarantees. Accurately measuring the flow rate poses challenges, particularly in low-head machines with heads below 50 m with shorter lengths intakes and developing flow [2]. Among various techniques, the pressure-time method (PTM) offers a relatively cost-effective and straightforward approach [3]. Based on the IEC-60041 standard, this method demonstrates an acceptable level of uncertainty within ± (1.5–2.0)% [4]. In addition to its applicability to hydropower, PTM has the potential for flow measurement in other applications.

According to the IEC-60041 [4], Eq. (1) can estimate the flow rate by integrating the measured differential pressure variation (Δp) between two cross-sections and modelling the viscous losses (Δp_f) during the deceleration of a fluid mass in a straight pipe with a consistent cross-section.

$$Q = \frac{A_c}{\rho L}\int_0^{t_f}\left(\Delta p + \Delta p_f\right)dt + q \qquad \text{Eq. 1}$$

Equation (1) involves several variables: Q, L, A_c, ρ and t_f and represents the initial flow rate before valve movement, the length between two cross-sections, the cross-sectional area, the water density, the final limit of integration and the leakage flow rate after valve closure. As stated by the IEC-60041 standard [3], the viscous pressure losses (ΔP_f) are assumed to be proportional to the flow rate square estimated by $\Delta P_f = KQ^2$. However, Adamkowski et al. [5] suggested an alternative premise where the pressure loss is related to the flow direction after valve closure and can be calculated by $\Delta P_f = KQ|Q|$. They showed that the suggested modification can decrease the deviation in flow measurement by around 1 %–3 % for different cases. For a better estimation of the friction factor in pressure-time methods, an unsteady formulation was used in different studies like Ref. [6–8].

According to the guidelines in IEC-60041 [3], the standard pressure-time method may not accurately measure flow rates in

* Corresponding author.
E-mail address: mehrdad.kalantar.neyestanaki@ltu.se (M.K. Neyestanaki).

https://doi.org/10.1016/j.flowmeasinst.2024.102535
Received 3 October 2023; Received in revised form 28 December 2023; Accepted 8 January 2024
Available online 17 January 2024

low-head machines. The IEC-60041 standard specifies certain limitations for the PTM. For instance, the distance between two cross-sections must be larger than 10 m, and the cross-sectional area between these measurement sections should be uniform without any significant irregularities. Furthermore, pressure taps must be placed at least two diameters away from any irregularity in the penstock. Additionally, the product of the measurement length (L) and average velocity in section (U) should be more than 50 m^2/s to guarantee accurate measurements. The purpose of these limitations is to guarantee the reliability of the PTM in flow rate measurement.

Numerous investigations have been done to determine the performances of the pressure-time method when applied beyond the mentioned limitation defined by the IEC-60041 standard. Jonsson et al. [6,9] examined the pressure-time method for straight pipes with a constant cross-section, with measuring lengths ranging from 3 to 10 m and product between velocity and length ($U \times L$) in the range of 3.5–50 m^2/s. These values are beyond the recommendations suggested in the IEC-60041 standard. Their measurements were satisfactory even for lengths below 4 m and $U \times L$ values below ten m^2/s, significantly lower than the IEC-60041 standard requirements. The highest mean deviation in flow rate estimation compared to the reference flow meter was for the smallest length ($L = 3$ m) and mean velocity ($U = 2.5$ m/s). By employing differential pressure sensors, the mean deviation was about 1 %, but when they used absolute pressure sensors, it was above 2 %. However, for measurements with larger U × L values, the mean deviation approached 0 %. This difference can be attributed to the uncertainty of the sensor's results in the lower range of the measurements. Moreover, it should be noted that smaller velocities and lengths caused larger errors in flow rate estimation. Lower velocities and distances result in lower pressure loss and pressure rise within a given closing timeframe. Consequently, the greater relative uncertainty associated with the measurement of the differential pressure using Eq. (1) contributes to an increased level of uncertainty in the estimated flow rate [10].

Adamkowski et al. [11] implemented the standard PTM on a curved penstock. They introduced a new relationship to take into account the geometric variations, incorporating a space-dependent geometry factor ($C = L/A_c$) as described in Eq. (2).

$$C = \int_0^L \frac{1}{A_c(x)} dx \quad \text{Eq. 2}$$

They proposed a new relation to account for changing the velocity profiles in a curved pipe [11]. Implementing mentioned modified geometry factor resulted in the variation of the estimated flow rate by approximately 0.45 %.

Ramdal et al. [12] studied the pressure-time method in the presence of a bend. They argued that the presence of two 45° bends caused a flow rate underestimation of approximately 1 %. However, a single 90° bend led to a more significant underestimation with a deviation of 8.5 % compared to the reference flow meter. This deviation is certainly the result of the Dean vortices present after the bend, which induces a radial pressure gradient. Therefore, the pressure at the taps is not representative of the mean pressure at the cross-sections considered. However, there is no previous detailed research that studies the effect of bends on the pressure-time method.

Adamkowski et al. [13] used computational fluid dynamics to estimate the friction coefficient for estimating viscous losses in a penstock with a variable cross-section. Equation (1) assumes a pipe with a constant cross-section that does not consider the dynamic pressure variation ($\Delta P_d = 0$). However, a new term must be considered for measurement sections with a variable cross-section or a secondary flow to estimate the dynamic pressure variation. They employed the energy equation and derived Eq. (3) to address this.

$$Q = \frac{1}{\rho C} \int_0^t \left(\Delta P_f + \Delta P + \Delta P_d\right) dt \quad \text{Eq. 3}$$

where ΔP_d is the dynamic pressure difference obtained by Eq. (4).

$$\Delta P_d = \alpha_2 \frac{\rho Q^2}{2A_2^2} - \alpha_1 \frac{\rho Q^2}{2A_1^2} \quad \text{Eq. 4}$$

The kinetic energy correction factor (α) is the ratio between the flux of kinetic energy calculated from the actual velocity (u) and the flux of kinetic energy calculated from the mean velocity (U). It is defined by Eq. (5) where A represents the cross-sectional area.

$$\alpha = \frac{1}{AU^3} \iint_A u^3 dA \quad \text{Eq. 5}$$

The constant value of 2 is utilised for the kinetic energy correction factor for laminar flows where the velocity gradient across the cross-section is greater than turbulence flow. In steady and developed turbulence flow conditions, a value of approximately 1.05 is suggested [14]. This lower value in turbulent flow is attributed to the flattening of the velocity profile across the section [15]. The mentioned kinetic energy correction factor values are applied to steady and fully developed flow conditions. However, a different value for the kinetic energy correction factor is expected in the case of a skewed velocity profile because the velocity profile deviates from the fully developed flattened one. A higher value of α is expected for non-uniform velocity distributions with the presence of vortices [16].

Neyestanaki et al. [10] compared the constant and quasi-steady assumptions for estimating pressure loss due to friction and dynamic pressure variation in a pipe with a variable cross-section. They observed that when a reducer was present in the pipe, the measurements exhibited significantly lower random uncertainty than half of those observed in pipes with a constant cross-section. This reduction in uncertainty was attributed to the higher differential pressure measured between the sections, leading to more accurate measurements. By applying the quasi-steady assumption for both the kinetic energy and friction factor coefficients, they reduced the deviation compared to the reference flow meter from −0.72 % to −0.42 %. This result was obtained under a steady and fully developed flow assumption. During unsteady conditions or in the developing flow region after the reducer, the values of the kinetic energy correction factor and friction factor coefficients may vary. To address this, the authors recommended utilising 3D computational fluid dynamics (CFD) simulations to account for the influence of developing flow on these coefficients [10]. CFD provides valuable insights into flow characteristics that are unattainable through experimental measurements. Numerous CFD investigations have studied the transient flow occurring when the pressure-time method is used: water hammer phenomenon and friction model have been a focus [2,13,17,18].

This approach provides a more comprehensive understanding of flow behaviour and improves the accuracy of flow rate measurements. No research studies on the kinetic energy correction factor values in developing conditions affected by bend during PTM are available. However, the presence of a bend is very frequent in penstock geometry for both low and medium-head hydropower.

Another analysed aspect is bends in pipes that introduce secondary flow known as Dean vortices. Shabani et al. [19] conducted an experimental study on turbulent flow in a 90° bend with a circular cross-section. The study revealed that the fluid near the outer wall of the bend experiences deceleration due to the unfavourable pressure gradient. Pressure measurements were monitored along three lines: the outer, middle, and inner bending radii. The results showed that the pressure varied significantly, even at a distance of 5 times the pipe diameter after the 90° bend.

In the context of the pressure-time method, the presence of bends can affect the symmetry of the pressure measurements. The skewed pressure profile observed in bends may lead to a value of the pressure at specific pressure taps different from the average pressure across the cross-section. Standard 1D PTM assumes constant pressure over the cross-

section. Therefore, the measured differential pressure from pressure taps in the pipe wall immediately after bends differs from the mean differential pressure in the pipe section, and boundary conditions may not be correct for the standard pressure-time method equation, leading to an inaccurate flow rate estimation. Therefore, special consideration should be given to the impact of bends on pressure measurement accuracy in PTM applications for the method to perform satisfactorily.

To investigate the flow characteristics in bends during the pressure-time method, 3D computational fluid dynamics can be employed. Utilising CFD offers several advantages, including the ability to study hydrodynamic forces and flow regimes in detail [29]. Additionally, CFD simulations provide a comprehensive distribution of all variables in any given section, which may not be readily available through experimental methods. By leveraging CFD, researchers can gain deeper insights into the flow behaviour in bends, enabling a more thorough understanding of the PTM and its accuracy in bend configurations.

This paper aims to investigate the application of the pressure-time method in the presence of a bend, specifically focusing on scenarios that deviate from the recommendations outlined in the IEC standards. The newly proposed methodology by Neyestanaki et al. [20] combining the 1D PTM based on an energy balance formulation and three-dimensional computational fluid dynamics (3D CFD) is used. The methodology is modified to take into account the new flow conditions.

To this end, a dedicated laboratory setup was designed and constructed to conduct experiments and evaluate the PTM's performance in such a configuration. In addition to the bend configuration, the study considers other factors beyond the IEC standards, such as shorter distances to irregularities. To gain a comprehensive understanding of the flow downstream of the bend during the PTM, 3D CFD simulations are performed. Combining experimental data and 3D CFD analysis aims to enhance the traditional 1D PTM methodology and extend its applicability to more complex flow scenarios. In particular, the radial pressure gradient and the kinetic energy correction factors and their effects on the pressure-time method are scrutinized. From this analysis, an update of the methodology proposed by Neyestanaki et al. [20] combining the 1D PTM and 3D CFD is proposed. The results are compared with those obtained using the standard 1D PTM, highlighting the effectiveness of the proposed updated methodology.

2. Materials and methods

2.1. Experimental setup

The current study is based on experimental data obtained from laboratory measurements. A test apparatus was designed and constructed at Luleå University of Technology, Sweden (LTU) to investigate the pressure-time method beyond the limitation of the IEC-60041 standard, such as small measurement lengths and developing flow irregularity in the pipe [2]. The experimental setup analyses flow characteristics similar to those in low-head turbine conditions. Other industrial flow measurement applications considering factors such as developing flows, short measurement lengths, and the presence of irregularities like bend and reducer can also be considered. Water flows via gravity in a stainless-steel pipeline between the mentioned tanks. The total head is 3.6 m, with a design flow rate of 15 l/s. The Reynolds number for this experiment is approximately $Re \approx 2.4 \times 10^4$ at the measurement sections considered in this paper. The stainless-steel pipe is assumed to have a roughness value of 0.0015 mm. The test section includes a 3.6 m vertical pipeline and 3 m horizontal pipe with a diameter of 150 mm, followed by a standard concentric reducer (DN 150 to DN 65) 255 mm long featuring a reducing angle of 9.46°. Subsequently, a 1 m pipe with a diameter of 65 mm is connected to a gate valve.

The valve is operated by a servo motor, allowing it to close within 1 s. The experimental setup incorporates one measurement section at the vertical pipe before the bend (section VA) and three sections after the bend in the horizontal line (sections HA, HB and HC), as illustrated in Fig. 1. At each measurement section, four pressure taps are installed around the circumference of the pipe at intervals of 90°. More details regarding the test rig can be found in Ref. [10] published by the authors.

In order to minimise uncertainty and enhance measurement precision, differential sensors are preferred over gauge sensors, primarily due to their narrower measurement range [9]. For the measurements in this study, a UNIK5000 differential sensor with a range of±35 kPa and an accuracy of ±0.04 % of full scale is employed. To ensure accurate readings, the sensors are calibrated utilising the reference pressure calibrator, Druck DPI 610.

The measurement of the reference flow rate is conducted using an Optiflux 2000F magnetic flowmeter, which offers a high level of accuracy with a tolerance of ±0.3 %. A data acquisition system provided by National Instruments (NI-9239) is utilised to capture the data. The system incorporates a 24-bit acquisition card and operates at a sampling frequency of 4 kHz.

The experiments are carried out with five different configurations mentioned in Table 1. Two conditions out of the IEC standard have been considered. The first configuration studies the effect of a 90° bend between two sections when applying the pressure-time method. The second one studies the effect of the presence of the bend upstream of the measurement section with a smaller distance than the IEC recommendation ($2 \times D$). The specification of the measurements, including the length between the sections and the distance to the bend upstream of the section, is mentioned in Table 1. For each set of measurement cases, ten experimental measurements were conducted. The random uncertainty associated with the pressure-time method measurements is determined by calculating the standard deviation of ten measurements using the following equation [21].

Table 1
Description of the different test cases.

Test case name	Inlet section	Outlet section	Elbow	Distance from the elbow to	
				Inlet section	Outlet section
VA-HA	VA	HA	yes	–	1.8 D
HA-HB	HA	HB	no	1.8 D	7.8 D
HB-HC	HB	HC	no	7.8 D	14.4 D
VA-HB	VA	HB	yes	–	7.8 D
HA-HC	HA	HC	no	7.8 D	14.4 D

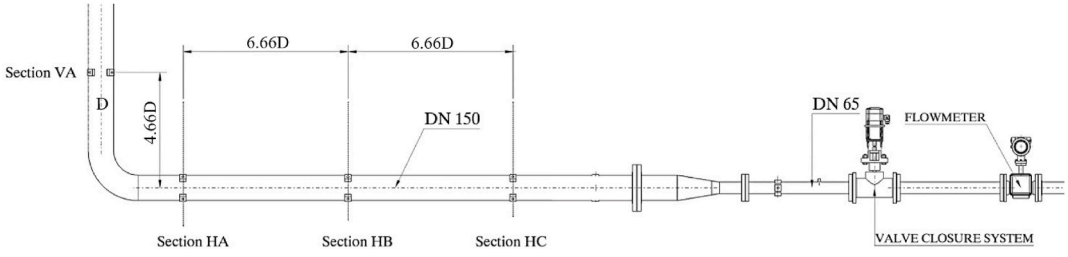

Fig. 1. Location of measurement sections.

$$\sigma_r = \left[\frac{1}{N-1}\sum_{i=1}^{N}(E_i - \overline{E})^2\right]^{0.5} \quad \text{Eq. 6}$$

The standard deviation of the measurements (σ_r) is calculated considering the number of experiments (N), the deviation value for each measurement (E_i) compared to the reference flow meter, and the mean of the deviations ($\overline{E}$). The systematic uncertainty associated with the test rig, as reported in Reference [13], is determined to be $\sigma_r = 0.1$ % using the Monte Carlo method or $\sigma_r = 0.24$ % using the Taylor series method. It should be noted that the systematic uncertainty is smaller than the random uncertainty mentioned in the study.

2.2. Flow rate calculation

In Eq. (3), three terms need to be measured or estimated. Pressure losses due to friction, ΔP_f, and dynamic pressure variations, ΔP_d, are estimated. The differential pressure, ΔP, is obtained from averaged pressure measurements between the sections considered. Pressure measurements are done at pressure taps, which may deviate from the average pressure at the considered sections because of the skewed pressure profile caused by the elbow. The 3D CFD can be employed to quantify this deviation in the pressure measurements to the average pressure. Moreover, 3D CFD are used to estimate the dynamic pressure variation at each section more accurately. Consequently, the flow rate can be estimated more accurately.

In the current study, a methodology is introduced, combining the 1D pressure-time method with 3D CFD to enhance the accuracy of pressure-time measurements in the presence of a bend. The time-varying flow rate obtained from the 1D pressure-time method is employed as an outlet boundary condition for the 3D CFD simulation. The primary objective of the 3D CFD simulation is to determine the velocity and pressure profile at the different sections of the test rig with similar flow conditions as the experiment, which are subsequently employed to determine the mean pressure and kinetic energy correction factor which will be later used in the 1D pressure-time method. An iterative loop with the 1D PTM and 3D CFD will be used to estimate the flow rate.

2.2.1. Flow rate calculation with 1D PTM

The flow rate is determined using Eq. (3) instead of Eq. (1), as dynamic pressure variation is expected because of the skewed profile and developing flow. As the pressure losses caused by friction are represented by $\Delta P_f(t) = KQ(t_t)|Q(t)|$, Eq. (3) is implicit, requiring an iterative loop to calculate the flow rate, Q(t). The iterative loop will persist until the flow rate is converged. The constant friction coefficient, K, is estimated based on experimental measurements under steady-state conditions using Eq. (7) before the valve movement [10].

$$K = \frac{-\Delta P(t_0) - \Delta P_d(t_0)}{Q(t_0)|Q(t_0)|} \quad \text{Eq. 7}$$

Here, $\Delta P_d(t_0)$, $Q(t_0)$, and $\Delta P(t_0)$ denote the dynamic pressure difference, flow rate, and measured differential pressure during the steady-state condition prior to the initiation of the valve movement. Approximately 40 s of measurement data were used to calculate the K value before the valve movement. The dynamic pressure variation estimated by Eq. (4) will be equal to zero in standard PTM when considering a constant value for the kinetic energy correction factor in 1D PTM.

The methodology described in Ref. [10] is employed to determine the integration endpoint for the pressure-time techniques using Eq. (3). In this approach, the flow rate is estimated based on various endpoints. The estimation process continues until the estimated flow rate variation becomes dampened and converges to a constant value. An illustration is presented in Fig. 2, where the transient flow rate, $Q(t)$, is determined using the standard PTM based on a sample of the measured differential pressure between sections HA and HB. In this method, the constant assumption is made for the friction coefficients and the kinetic energy correction factor. Subsequently, the time-dependent flow rate obtained from the previous step is employed as a boundary condition for the 3D CFD simulation.

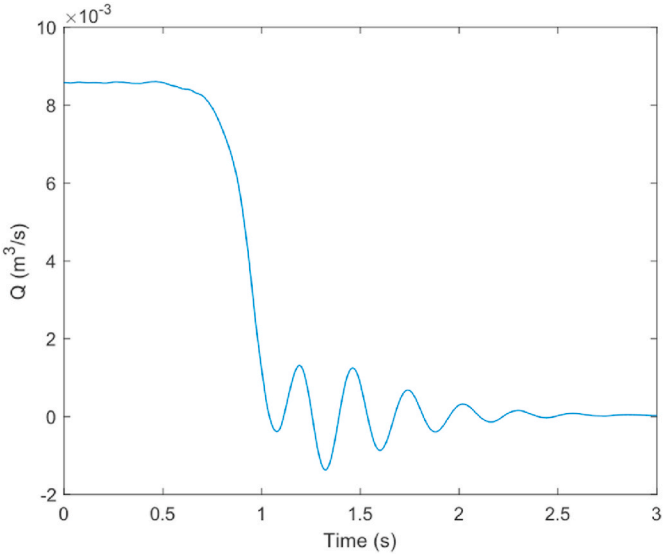

Fig. 2. Transient flowrate estimated using the 1D pressure time method and experimental measurement.

2.3. Mathematical modelling

The complete transient of the pressure-time method is simulated using 3D CFD, incorporating the 3D geometry of the experimental setup. The simulation utilises the continuity and momentum equations to model the behaviour of the incompressible, isothermal, and turbulent fluid flow over time. The governing equations for the time-dependent, incompressible, turbulent flow are described as follows.

$$\frac{\partial(\rho U_j)}{\partial x_j} = 0 \quad \text{Eq. 8}$$

$$\rho\frac{\partial(U_i)}{\partial t} + \rho\frac{\partial(U_j U_i)}{\partial x_j} = -\frac{\partial p}{\partial x_i} + \frac{\partial}{\partial x_j}\left(\mu\frac{\partial U_i}{\partial x_j} - \rho\overline{u_i u_j}\right) \quad \text{Eq. 9}$$

In order to accurately capture the oscillations occurring after valve closure, the influence of compressibility needs to be taken into account [22]. However, the density variation is considered negligible, as the water hammer wave associated with the valve closure is simulated using the 1D model, which is applied as the boundary condition. The low Reynolds k-ω SST turbulence model from Menter [23] is employed to approximate the turbulence shear stress term, $-\rho\overline{u_i u_j}$. This particular turbulence model, the SST k-ω, is widely acknowledged for its enhanced accuracy in predicting fluid flow in the near-wall region at low Reynolds numbers. In this model, the omega formulation is utilised near the walls, while the k-ε formulation is applied further away from the walls [24]. The value of Y^+ is considered to be around 1, indicating that the near-wall mesh resolution is appropriately captured.

The temperature variation is disregarded in the analysis. The coupled finite volume equations of motion are solved using ANSYS-Fluent. The pressure field is computed using the semi-implicit method for the pressure-linked equations (SIMPLE) algorithm. The third-order monotonic upwind scheme is utilised to discretise the nonlinear convective terms in all transport equations, following similar approaches employed in previous studies such as Refs. [2,22,25,26]. The first-order implicit scheme is employed to approximate the time derivative terms. Convergence of the variables is deemed achieved when the root-mean-square (RMS) residual levels reach a threshold of 10^{-5}.

2.3.1. Boundary condition

In order to simplify the 3D CFD simulations, a transient flow rate is imposed as an outlet boundary condition instead of explicitly modelling the valve closure [26]. This approach is adopted to avoid the additional computational time required for simulating the valve closure. The entire upstream geometry of the valve is included in the simulation to account for the influence of the developing flow. The flow domain considered in the simulation is presented in Fig. 3. During the simulation, the total pressure is considered as the boundary condition at the inlet. The transient flow rate Q(t) estimated from the 1D PTM (Fig. 2), is employed as the outlet boundary condition for the 3D CFD simulation. A converged steady state is achieved with an initial mass flow outlet to establish the initial condition. There is a minor oscillation in the flow rate after valve closure showed in Fig. 2. This oscillation, nevertheless, might not exactly reflect the physical behaviour since after the valve closes, the flow rate at the valve is zero.

Three timesteps, 0.01 s, 0.005 and 0.002 s were applied to the simulation. The differential pressure obtained from CFD is not dependent on the time step size considered. Therefore, a timestep 0.01 s is used for the simulations. The time step size of 0.01s used in this study is 100 times larger than the time step typically employed for modelling valve closure, as demonstrated in previous studies (Refs. [2,25–27]). This indicates a significant reduction in computational cost for the presented 3D CFD simulation compared to other methods that explicitly model valve closure. The simulation encountered divergence issues for larger time steps due to rapid velocity variations over short intervals near the time step.

2.4. New flow rate calculation method

The 3D CFD results are utilised to update the 1D pressure-time method by modifying the terms within Eq. (3). During the transient 3D CFD simulation, velocity and pressure profiles are monitored at the considered measurement sections. From these simulations, the deviation of the pressure measurements at the pressure taps from the mean value at the section caused by the skewed pressure profile after the bend is quantified. Moreover, the kinetic energy correction factor variation is estimated and then used. The updated value of the transient flow rate is then applied as input for the subsequent iteration of the CFD simulation. This iterative loop continues until convergence is achieved. The residual on the variation of the estimated flow rate is considered as the convergence criteria. A flowchart illustrating the steps is provided in Fig. 4 for a comprehensive understanding of the calculation process.

The methodology was applied to a sample of experimental measurement between sections HA-HB. The transient flow rate in Fig. 2, calculated by the 1D PTM was applied as the boundary condition for the 3D CFD simulation. Differential pressure at the location of pressure taps of section HA-HB from 3D CFD compared with the same experimental differential pressure measurement between sections HA-HB are shown in Fig. 5. The good agreement observed in Fig. 5 confirms the validity of the proposed method. This demonstrates that 3D CFD can effectively

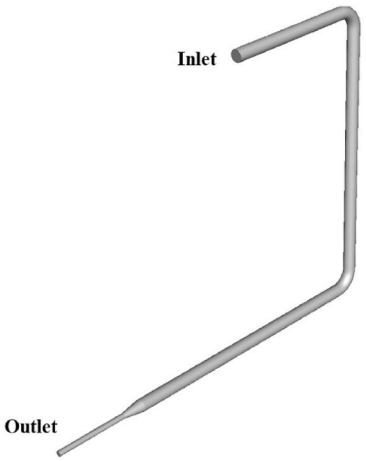

Fig. 3. 3D domain for CFD simulation.

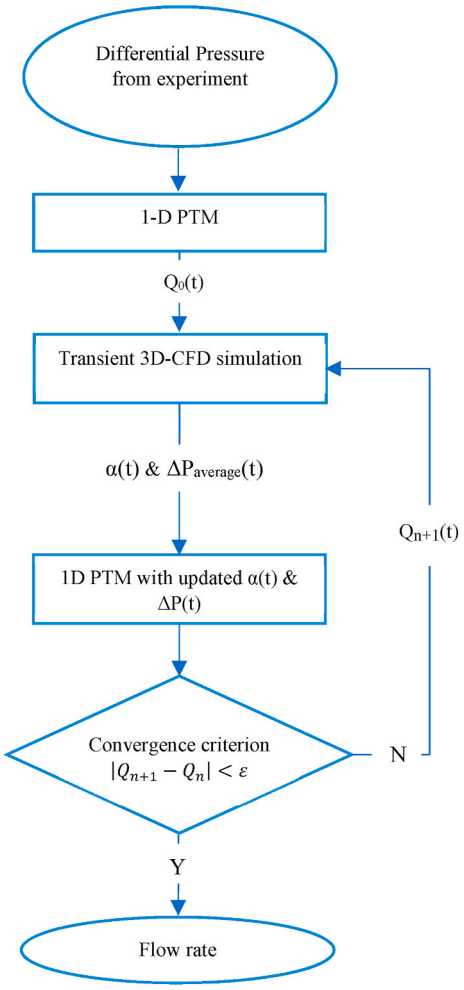

Fig. 4. Flowchart for the iterative loop combining the 1D PTM and 3D CFD.

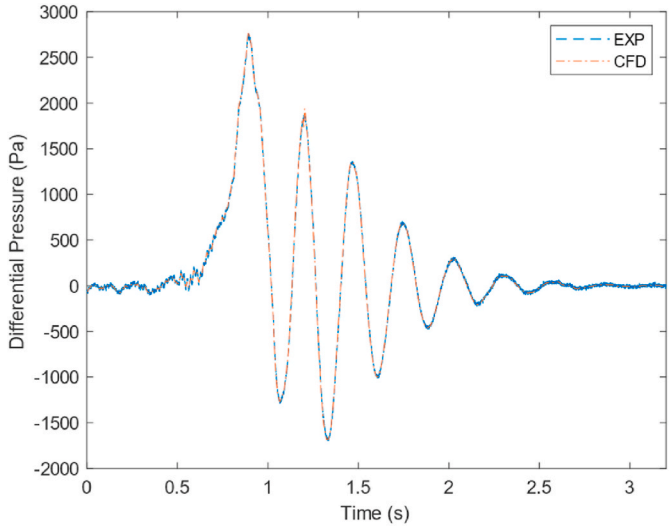

Fig. 5. Experimental and 3D CFD numerical differential pressure between section HA-HB at the location of the pressure taps.

replicate flow conditions similar to those observed in considered experimental setups.

3. Results and discussion

3.1. Experimental results with standard 1D PTM

Fig. 6 shows the mean deviation of the measurement using the standard PTM compared to the reference flow rate and the random uncertainty with 95 % confidence ($\pm 2\sigma_r$) for five cases of measurements. Ten measurements have been considered for each case with the specification mentioned in Table 1 to calculate random uncertainty. A constant value for the kinetic energy correction factor is applied on the measured differential pressure. The geometry factor is calculated using Eq. (2), and accounting for the changing velocity profiles in a curved pipe (introduced by Ref. [11]) is negligible in our cases (less than 0.05 %). The reason could be related to the length of the straight pipe before and after the bend. The results of two cases in which the bend was located between two sections of the measurements (VA-HA and VA-HB) are shown in Fig. 6-right, and the three cases in which the bend was located upstream of the first section of the measurements (HA-HB, HB-HC and HA-HC) are shown in Fig. 6-left.

After the bend, the flow is non-uniform and developing with Dean vortices. Measured differential pressure from pressure taps deviated from the average pressure in the pipe sections and lead to a deviation of the measured pressure compared to the mean pressure. For measurement in which the first section is located after the elbow (HA-HB, HB-HC and HA-HC), the measurement with the standard PTM leads to a negative deviation compared to the reference flow rate. This underestimation of the flow rate will lead to an overestimation of the turbine efficiency. The measurements between sections HA-HB, where the first section is closer to the bend, result in a higher deviation of −0.74 % compared to HB-HC, with a mean deviation of −0.39 %. Measurement between sections HA-HC with the length of 2 m has a similar negative deviation of −0.55 % but with a lower random uncertainty, $\sigma = 0.3$ %. The reason is the higher measured differential pressure compared to the uncertainty of the sensor, which leads to lower random uncertainty. For measurements in which the bend is located between two sections, the standard PTM results in a positive deviation in the flow rate measurement. Measurements between sections VA-HA with a length of 1 m have a positive mean deviation of 1.30 %. Measurements between sections VA-HB with a length of 2 m have a smaller positive mean deviation of 0.32 %.

Measurements between sections VA-HA have the highest random uncertainty $\sigma = 0.78$ %, and the reason is attributed to the transient secondary flow, which can differ between the measurements. The lowest random uncertainty for the measurements with a length of 1 m is for the measurements between sections HB-HC ($\sigma = 0.47$ %) where the sections are far from the bend.

It is challenging to justify the reason for the negative mean deviation of the measurements in Fig. 6-left and the positive mean deviation of measurement in Fig. 6-right without some flow details. However, detailed information on the pressure and velocity profile at each section from 3D CFD can help find the reason for negative mean deviation for measurement cases with the presence of the bend upstream of the first measurement section and positive deviation for cases with the presence of bend between two measurement sections.

3.2. CFD result

This study proposes to use 3D CFD to improve the accuracy of the 1D PTM. Firstly, three-dimensional CFD is employed to check if there is any deviation in the measurement of the mean ΔP at the pressure taps compared to the mean pressure of the sections considered induced by the skewed pressure profile after the bend. Then, 3D CFD is used to estimate ΔP_d more accurately, in particular the kinetic energy correction factor. For ΔP_f, the relation $\Delta P_f = KQ|Q|$ sensitive to the flow direction [10] is used where K is obtained from the experimental measurements. The reason is the difficulty of 3D CFD to capture accurately the losses.

3.2.1. Differential pressure

Fig. 7 shows the pressure distribution and surface streamlines at different sections after the bend from steady-state simulation. The distance of the sections to the bend is shown based on the pipe's diameter. The skewed pressure is clearly seen in both pressure contour and surface

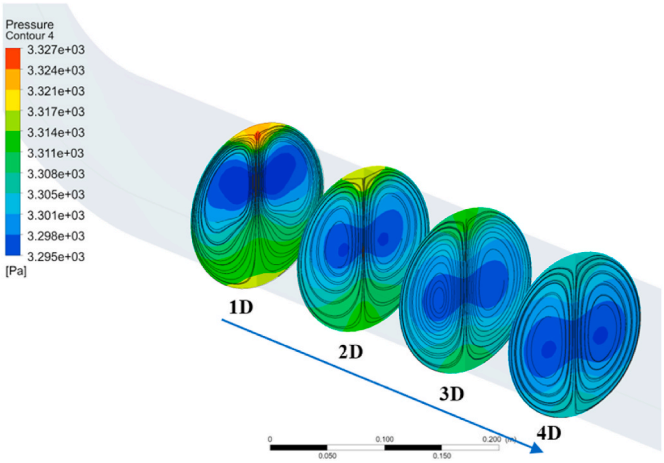

Fig. 7. Pressure distribution and surface streamlines at different sections after the bend from steady-state simulation.

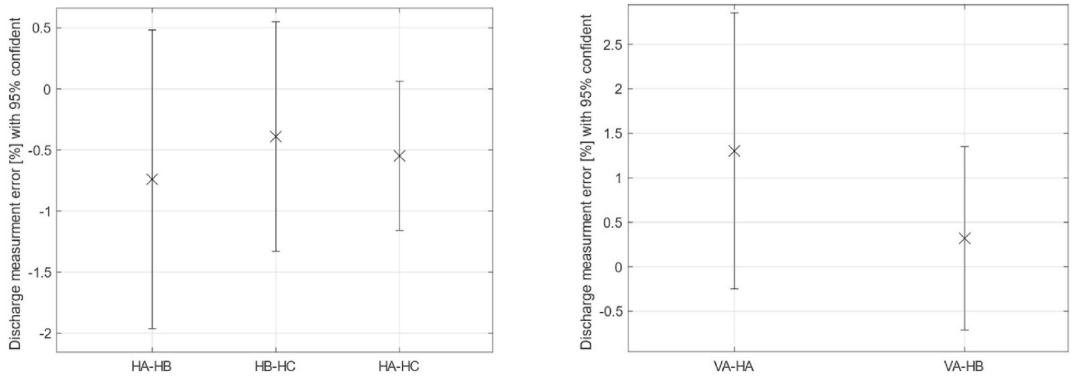

Fig. 6. Mean deviation of the estimated flow rate compared to the reference flow meter for 5 cases, left: between sections HA- HB, HB-HC and HA-HC), right: between sections VA- HA and VA-HB. The bars represent the random uncertainty at 95 % confidence.

streamlines. It can be observed that the differential pressure from pressure taps is not equal to the average pressure in the pipe section and leads to a deviation in the flow rate estimation with the standard PTM compared to the reference flow meter. The intensity of Dean vortices decreases further away from the bend. The deviation of pressures on the walls compared to the mean cross-sectional pressures for different sections normalised by the dynamic pressure term $((P_{Tap} - P_{cross\text{-}section})/(½ \rho U^2) \times 100)$ is presented in Fig. 8. The pressure taps are located at angles of 45, 135, 225 and 315°. The pressure measurement at section HA has a 10 % (10–15 Pa) deviation from the dynamic pressure. However, for section HB with a distance larger than 2 × D (as recommended in IEC), the deviation decreases to 3 %. For section HC, the deviation is less than 1 % and for section VA (before the bend), the deviation is approximately 0 %.

The methodology presented in Fig. 4 is applied to the same sample of the experimental measurements between sections HA-HB. The pressure variation at four the sections, VA, HA, HB and HC, is monitored during the transient simulation. The normalised pressure deviation $(\Delta P_{Tap} - \Delta P_{Average})/\Delta P_{Average}$ is defined to quantify the deviation of the measured differential pressure from the pressure taps to the average pressure at the pipe sections. $\Delta P_{Average}$ is the average differential pressure between two sections obtained from 3D CFD. ΔP_{Tap} is the differential pressure between two sections by getting the average of the four pressure taps at each section obtained from 3D CFD, which matches the experimental measurement locations. The variation of the normalised pressure deviation during the PTM is presented in Fig. 9. Later, $(\Delta P_{Tap} - \Delta P_{Average})_{CFD}$ will be subtracted from the measured differential data at the pressure taps to eliminate the deviation in the pressure measurement.

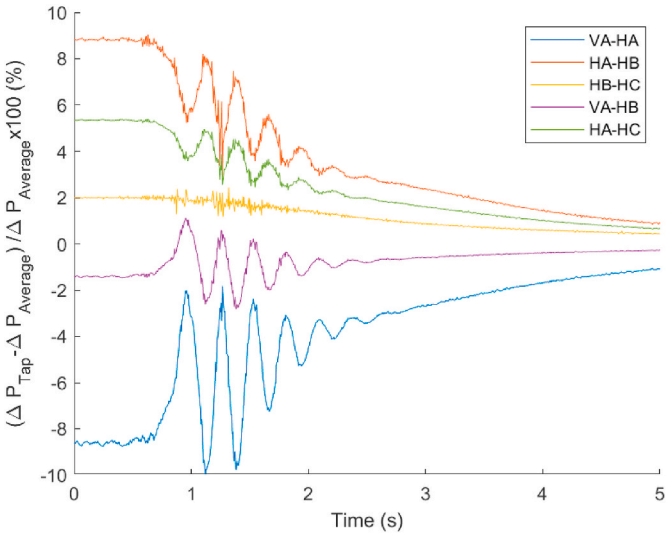

Fig. 9. Normalised deviation of pressure measurement at four sections.

The CFD results presented in Fig. 9 can clarify the experimental deviation of the flow rate obtained from the 1D standard PTM shown in Fig. 6. If the bend is located between two measurement sections, the pressure measurement leads to an underestimation of the differential pressure. For example, the experimental measurement between sections VA and HA underestimated the differential pressure by −10 to −2%, leading to a lower value (higher magnitude) for estimating the pressure

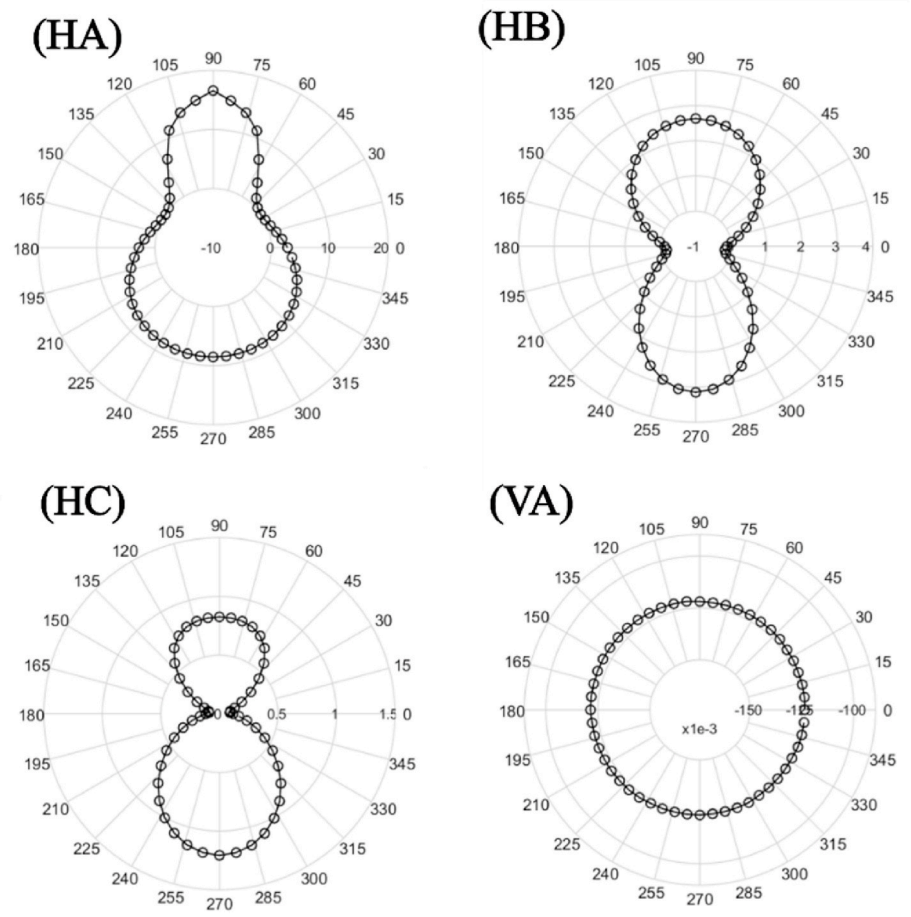

Fig. 8. Normalised deviation of the pressures on the walls compared to the mean cross-sectional pressures in % of the dynamic pressure for different sections (HA, HB, HC and VA).

loss before the valve movement by Eq. (6). This leads to an overestimation of the area between the differential pressure and the pressure loss, and, consequently, an overestimation of the flow rate. This explains the overestimation of the flow rate for the measurements between sections VA-HA and VA-HB by the standard PTM shown in Fig. 6-right.

Similarly, a positive deviation of the pressure measurements at the taps is observed when the elbow is upstream of the first measurement section. Therefore, measurements for the cases HA-HB, HB-HC, and HA-HC have an overestimated differential pressure, leading to a larger value (lower magnitude) to estimate pressure loss. This leads to an underestimation of the area between the differential pressure and the pressure loss and, consequently, an underestimation of the flow rate. This is a reason for underestimating the flow rate for measurement shown in Fig. 6-left.

Measurement of the case HB-HC has less deviation to estimate the average differential pressure from the experimental measurement at the pressure taps compared to case HA-HB as the distance between the sections is increased. This explains that there is a lower negative deviation in the estimation of the flow rate for this set of measurements. For measurements for the cases VA-HB and HA-HC, as the length is larger (2 m), the normalised deviation is smaller (Fig. 9), resulting in a smaller mean deviation than the measurements for the cases VA-HA and HA-HB in the flow rate obtained with the standard PTM.

3.2.2. Dynamic pressure

Another parameter affecting the results is the dynamic pressure variation. The variation of the kinetic energy coefficient depends on the velocity variation at the cross-section, as defined in Eq. (5). Fig. 10 illustrates the velocity distribution and surface streamlines at sections HA before and after valve closure at t = 3 s. In the steady-state condition before valve closure, the skewed velocity caused by the bend is clearly observed at section HA, leading to higher values of α compared to other sections. After valve closure, a lower mean velocity value and a higher velocity gradient in the cross-section will result in a higher kinetic energy correction factor compared to steady state condition.

The variation of the kinetic energy correction factor at four sections is monitored during the valve closure and presented in Fig. 11. For section VA where the flow is expected to be fully developed, the value is close to 1.05 before the valve movement, similar to the value mentioned in Ref. [14]. For section HA, a higher value of the kinetic energy correction factor is predicted, which could be related to the skewed velocity profile. For sections HB and HC, the value is closer to section VA as the distance to the bend increases, and the flow becomes comparable

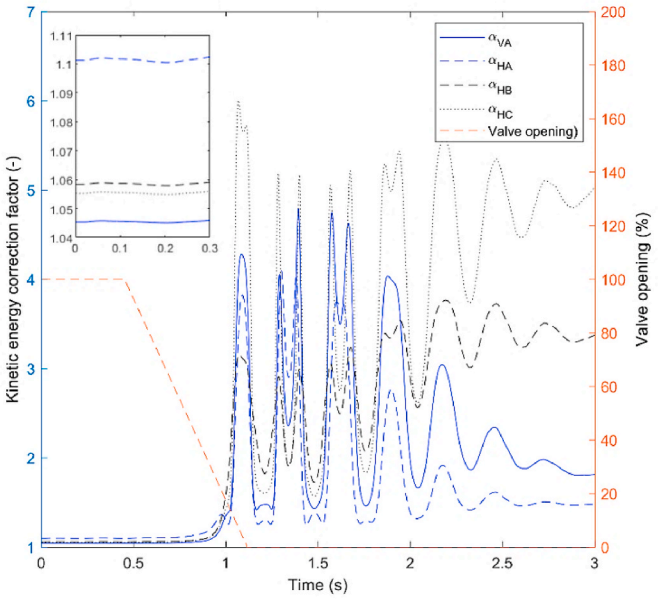

Fig. 11. Variation of the kinetic energy correction at four sections during PTM.

to the fully developed flow. The kinetic energy correction factor is expected to increase during the transient conditions as the mean velocity decreases towards zero. However, the difference between the different sections cannot be clearly established as there is a lack of studies in this area. The reason for the higher value of 5 at section HC compared to other sections (values close to 4) may be related to the vortexes after valve closure. After valve closure, the water hammer wave goes through the piping and section HC is closer to the reducer in the test rig.

The variation of $\Delta P_f + \Delta P_d$ considering the constant assumption of the kinetic energy correction factor (standard 1D PTM) and variation based on 3D CFD data (presented methodology) is presented in Fig. 12 for the same measurement sample between HA-HB.

For the estimation of ΔP_f, $\Delta P_f = KQ|Q|$ is used where K is obtained using Eq. (7). K depends on the variation of the differential pressure and dynamic pressure before valve movement. For the variation ΔP_d, two assumptions for the variation of the kinetic energy correction factor are considered: constant and variable kinetic energy correction factor from 3D CFD data. The curve obtained for a constant α represents only the

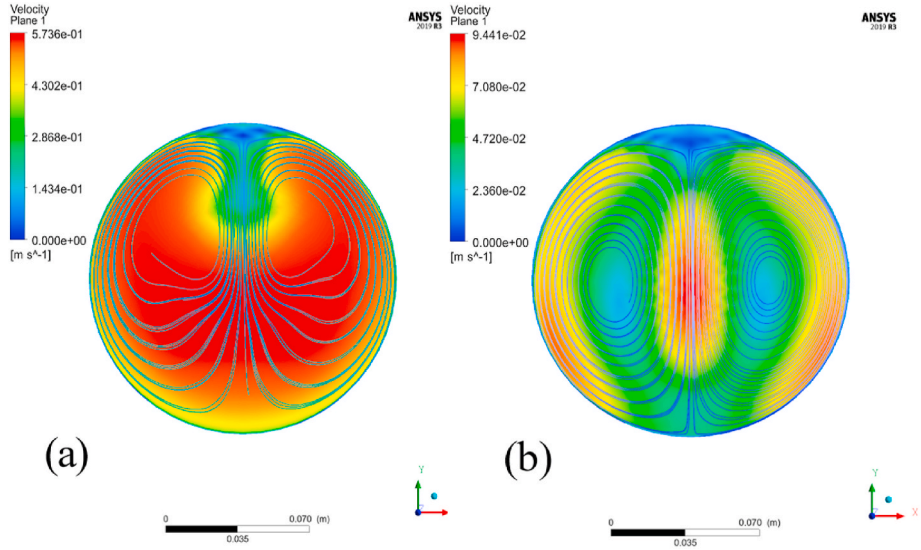

Fig. 10. Velocity magnitude distribution and surface streamlines at HA sections (a) before and (b) after the valve closure (t = 3 s).

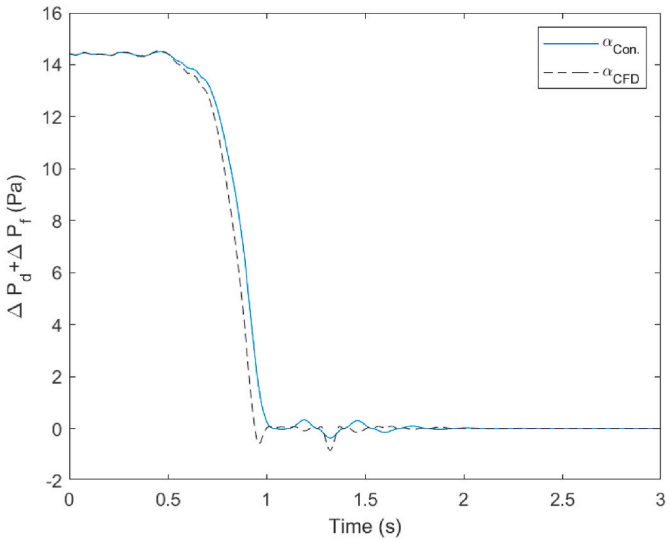

Fig. 12. Variation of $\Delta P_f + \Delta P_d$ with a constant value of kinetic energy correction factor and a time-dependent value predicted by 3D CFD.

variation of the pressure losses as the variation of the dynamic pressure is null. As shown in Fig. 13, before the valve movement, similar values are observed, equal to the measured differential pressure. However, the constant kinetic energy correction factor assumption leads to an overestimation compared to CFD during the valve closure. Therefore, the constant assumption leads to an overestimation of the area between the differential pressure and $\Delta P_f + \Delta P_d$, and consequently, overestimation of the flow rate. This effect is quantified in Fig. 14 and discussed.

3.3. Expansion of PTM by 3D CFD

The methodology is further applied to the experimental test case HA-HB. The variation of the kinetic energy coefficient and deviation of the pressure measurement at the pressure tap compared to the mean pressure are monitored during the transient simulation. The obtained data is applied to adjust the terms in the 1D PTM method.

The flowchart presented in Fig. 4 is applied for two iterations. The variation of the estimated flow rate deviation compared to the reference flow meter function of different endpoints is shown in Fig. 13. The first

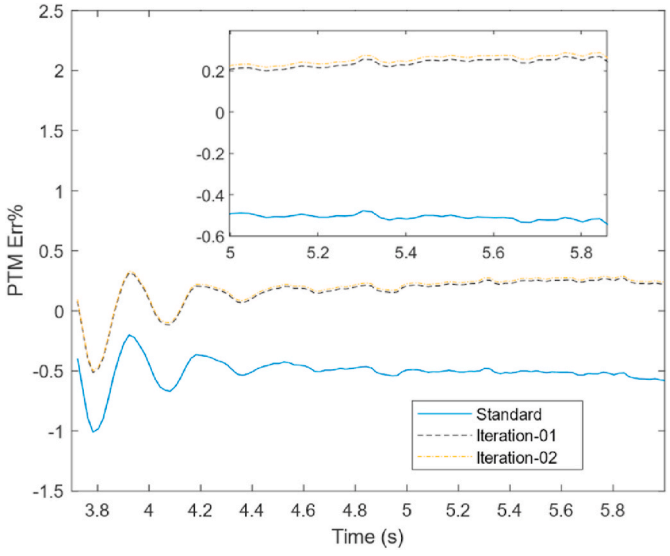

Fig. 13. Variation of the deviation compared to the reference flow meter for two iterations function of endpoints based on modified PTM.

and second iterations have similar values for the flow rate and deviation. Both iterations differ by less than 0.02 %. Therefore, the solution is assumed to converge after the first iteration. The adjustment to the updated flow rate is 0.6 %. The slight variation in flow rate will not affect the correction of the differential pressure measured at the taps and estimated dynamic pressure variation with the flow rate adjustment compared to the previous iteration. This estimated initial flow rate change will not lead to significant variation for the second iteration. Therefore, the second iteration is not necessary.

The methodology is applied to a sample of each measurement set mentioned in Table 1, the one close to the mean deviation. The estimated flow rate is compared to the reference flow rate function of different endpoints and presented in Fig. 14. The effect of applying the proposed methodology involving a pressure correction at the pressure taps and the dynamic pressure correction factor is presented. The results show the deviation of the pressure measurement from the pressure taps has a more significant effect on the flow rate estimation than the dynamic pressure variation for all cases. Applying the methodology for measurement where the bend is located upstream of the first section led to an increment in the estimated flow rate. The deviation is changed by around +0.85 % for measurement between sections HA and HB. For measurement between sections HA and HC with the larger length, applying the methodology has a smaller effect with a change of +0.3 % of the deviation. For measurement between sections HB and HC with a higher distance to the bend, the change in deviation is lower compared to other cases, around +0.25 %. This trend can be justified by the deviation of the pressure measurement at the pressure taps compared to the average pressure shown in Fig. 9.

Applying the methodology for measurements where the bend is located between two sections decreases the estimated flow rate. For measurement between sections VA and HA with the highest uncertainty of random measurement, lead to a change of deviation around −1.8 %. For measurement between sections HA and HC with a longer a length has a smaller effect with a change of deviation around −0.6 %.

Moreover, the effect of considering the kinetic energy coefficient is smaller than the effect of pressure measurement at the location of the taps with changes of the deviation around 0.2 % or less. Fig. 12 is used as a sample to check the effect of dynamic pressure variation, and it can be done for other cases, too.

3.4. Repeatability

The methodology presented in Fig. 4 was applied to all the cases presented in Table 1. For each case, three measurements were chosen as a function of their deviation from the reference flow rate using the 1D PTM. These measurements correspond to the lowest, closest and largest deviation from the mean.

It is observed that the magnitude of the change in deviation is similar for the three measurements of each case in Table 1. The difference in the flow rate estimation between the different measurements of the same case is below ±0.05 %. The mean deviation of the 1D PTM is adjusted to the modified PTM (presented methodology) with the change in the deviation obtained from the 3 cases as it is constant.

Fig. 15 shows the mean deviation using the 1D PTM and modified PTM presented in the paper. The uncertainty at 95 % confidence showed just for results based on standard PTM as the uncertainty is constant whether standard or modified PTM is applied to the data.

The results show the mean deviation decreased significantly for all cases. For four cases with random uncertainty of 0.6 % or less, including the cases HB-HC, HA-HC, VA-HB and HA-HB, the mean deviation after applying the methodology reached a range of ±0.15 % which is in the range of systematic uncertainty of reference flow flowmeter. For measurement between sections VA-HB, with the highest random uncertainty of 0.78 % and higher initial mean deviation of 1.3 %, after applying the methodology, the mean deviation reached −0.4 %. The error introduced by the elbow is outside the 95 % confidence interval, further

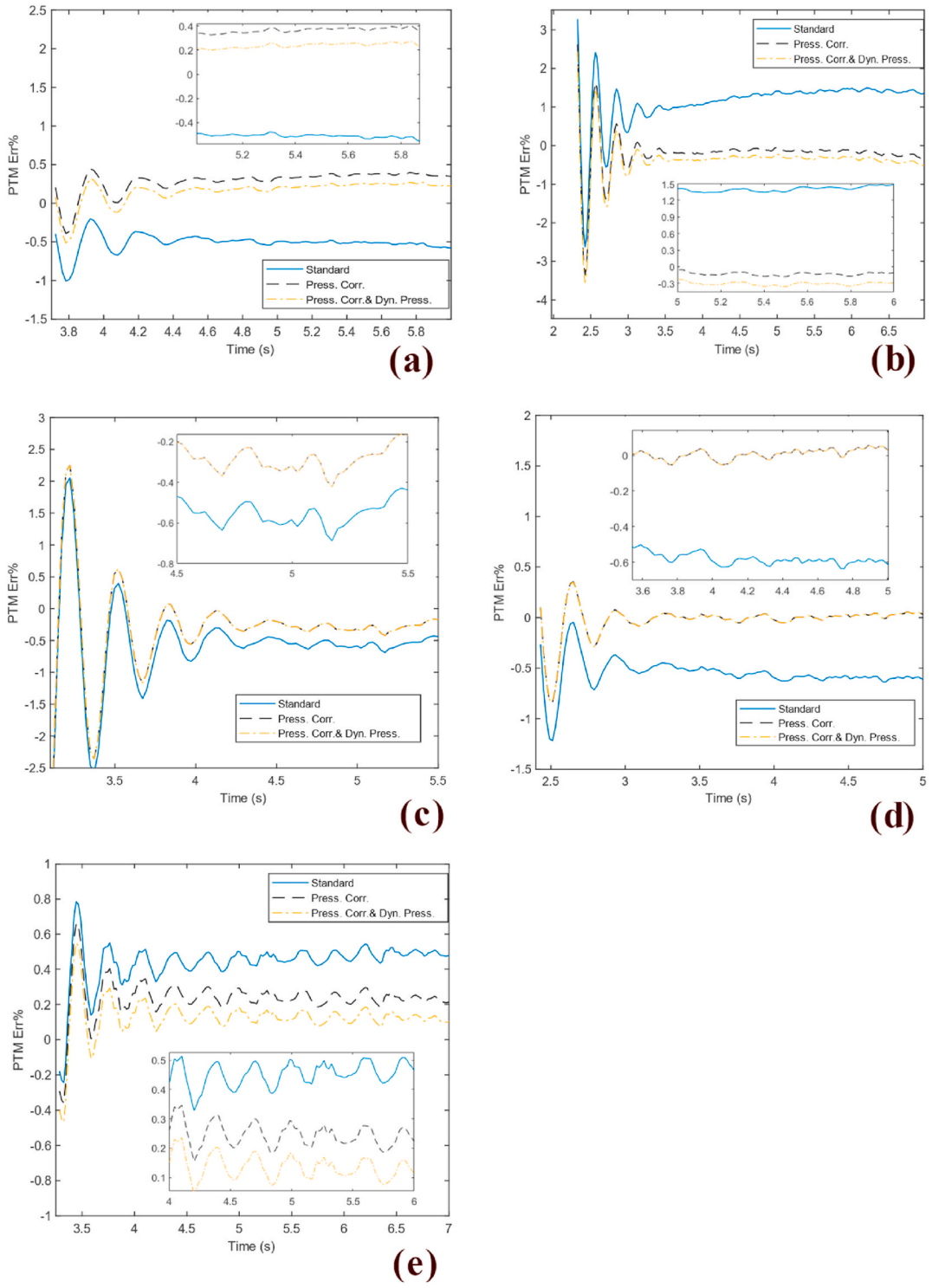

Fig. 14. Flowrate deviation compared to the reference flow meterfunction of endpoint for all cases (a) HA-HB, (b) VA-HA, (c) HB-HC, (d) HA-HC, (e) VH-HB

emphasising the importance of including 3D CFD. The reason is the large deviation of the pressure measurement at the pressure taps with the mean cross-sectional pressure, see Fig. 8.

The methodology has successfully been applied to canonical test cases such as contraction [28] and 90° bend. The applicability of the method should be extended to other geometries but also cases with free surface flow inlet to the pipe to mimic low head hydropower plants.

4. Conclusion

This research paper investigates the utilisation of the pressure-time method beyond the recommended guidelines of the IEC standard, particularly in the presence of a bend between the two measurement sections or in close proximity to one. Experimental measurements were conducted for different arrangements outside the IEC standard. The results from the standard 1D PTM show that a bend between the measurement section leads to an overestimation of the flow rate, and a bend upstream of the first measurement section leads to an underestimation

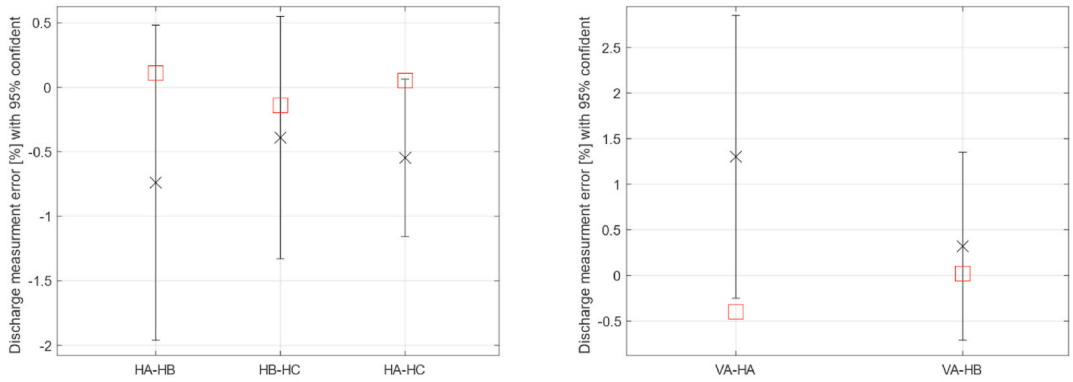

Fig. 15. Flowrate deviation for all cases; × represents the mean deviation of the experimental measurement with 1D PTM, □ represents the mean deviation with 3D CFD methodology. The bars represent the uncertainty at 95 % confidence based on standard PTM.

of the flow rate.

A combination of 3D CFD and 1D PTM is employed to improve the accuracy of the flow rate estimation. Initially, the one-dimensional pressure-time method is utilised to calculate the transient flow rate, which serves as the outlet boundary conditions for the subsequent 3D CFD simulation. The 3D CFD simulation is conducted to obtain detailed pressure and velocity profiles in different sections of the test rig under conditions similar to each experimental measurement. The obtained pressure and velocity profile information is then utilised to determine the deviation of the pressure measurement at pressure taps affected by the bend and the kinetic energy correction factor for each section, improving the accuracy of the 1D pressure-time method. Applying the kinetic energy correction factor changes the deviation of flow measurements by around 0.2 % or less; however, the results of applying the mean pressure at each section from the 3D CFD change the deviation by more than 1 % for some cases.

The findings of this study indicate that the methodology enhances the accuracy of the method, and the deviation of the measurement compared to the reference flow meter is decreased to the range of random uncertainty of measurement. Therefore, it is suggested to apply the methodology based on the real geometry of the penstock for low and medium hydropower turbines.

CRediT authorship contribution statement

Mehrdad Kalantar Neyestanaki: Conceptualization, Data curation, Investigation, Methodology, Software, Validation, Visualization, Writing – original draft. **Georgiana Dunca:** Methodology, Supervision, Writing – review & editing. **Pontus Jonsson:** Supervision, Writing – review & editing. **Michel J. Cervantes:** Funding acquisition, Investigation, Methodology, Project administration, Resources, Supervision.

Declaration of competing interest

The authors declare that they have no known competing financial interests or personal relationships that could have appeared to influence the work reported in this paper.

Data availability

Data will be made available on request.

Acknowledgement

The research presented was carried out as a part of “Swedish Hydropower Centre-SVC” has been established by the Swedish Energy Agency, Elforsk and Svenska Kraftnät, together with the Luleå University of Technology, The Royal Institute of Technology, Chalmers University of Technology, and Uppsala University.

References

[1] Renewable Energy, Our World in Data, 2019.
[2] S. Saemi, M. Raisee, M.J. Cervantes, A. Nourbakhsh, Numerical investigation of the pressure-time method considering pipe with variable cross section, J.Fluid. Eng Trans ASME 140 (2018), https://doi.org/10.1115/1.4040718.
[3] B. Baidar, J. Nicolle, C. Trivedi, M.J. Cervantes, Winter-kennedy Method in Hydraulic Discharge Measurement: Problems and Challenges, Proceedings of the IGHEM, 2016.
[4] IEC 60041, I. Field Acceptance Tests to Determine the Hydraulic Performance of Hydraulic Turbines, Storage Pumps and Pump-Turbines. International Standard, 1991.
[5] A. Adamkowski, W. Janicki, Selected problems in calculation procedures for the gibson discharge measurement method, in: Proceedings of the GHEM, Roorkee, India, 2010.
[6] P.P. Jonsson, M.J. Cervantes, M. Finnström, Numerical investigation of the gibson’s method : effects of connecting tubing, in: 2nd IAHR International Meeting of the Workgroup on Cavitation and Dynamic Problems in Hydraulic Machinery and Systems, 2007.
[7] P.P. Jonsson, J. Ramdal, M.J. Cervantes, Development of the gibson method-unsteady friction, Flow Meas. Instrum. 23 (2012) 19–25, https://doi.org/10.1016/j.flowmeasinst.2011.12.008.
[8] G. Dunca, R.G. Iovanel, D.M. Bucur, M.J. Cervantes, On the use of the water hammer equations with time dependent friction during a valve closure, for discharge estimation, J. Appl. Fluid Mech. 9 (2016) 2427–2434, https://doi.org/10.18869/acadpub.jafm.68.236.25332.
[9] P.P. Jonsson, J. Ramdal, M.J. Cervantes, A. Getz, Experimental investigation of the gibson’s method outside standard, in: Proceedings of the 24th Symposium on Hydraulic Machinery and Systems, IAHR, 2009.
[10] M.K. Neyestanaki, G. Dunca, P. Jonsson, M.J. Cervantes, Experimental study of the pressure-time method with potential application for low-head hydropower, J. Fluid Eng. 145 (2023) 1–45, https://doi.org/10.1115/1.4062090.
[11] A. Adamkowski, Z. Krzemianowski, W. Janicki, Improved discharge measurement using the pressure-time method in a hydropower plant curved penstock, J. Eng. Gas Turbines Power 131 (2009), https://doi.org/10.1115/1.3078794.
[12] J. Ramdal, P. Jonsson, T. Nielsen, Influence from bends on a pressure-time measurement, IOP Conf. Ser. Earth Environ. Sci. 12 (2010) 012078, https://doi.org/10.1088/1755-1315/12/1/012078.
[13] A. Adamkowski, W. Janicki, M. Lewandowski, Measurements of discharge through a pump-turbine in both flow directions using volumetric gauging and pressure-time methods, Energies 13 (2020), https://doi.org/10.3390/en13184706.
[14] Y.A. Çengel, J.M. Cimbala, Fluid Mechanics A Fundamental Approach, 2018.
[15] J.B. Franzini, E.John Finnemore, R.L. Daugherty, L. Robert, Fluid Mechanics with Engineering Applications, 1997, p. 807.
[16] F.M. Henderson, M. Francis, Open Channel Flow, 1966, p. 522.
[17] S. Saemi, L.R.J. Sundström, M.J. Cervantes, M. Raisee, Evaluation of transient effects in the pressure-time method, Flow Meas. Instrum. 68 (2019), https://doi.org/10.1016/j.flowmeasinst.2019.101581.
[18] L.R.J. Sundstrom, S. Saemi, M. Raisee, M.J. Cervantes, Improved frictional modeling for the pressure-time method, Flow Meas. Instrum. 69 (2019), https://doi.org/10.1016/j.flowmeasinst.2019.101604.
[19] S. Shabani, A.A. Abedini, A. Mohammadtabar, The effect of the pipe bending angle on the pressure losses vane elbow pipes, Asian Rev. Civil Eng. 8 (2019), https://doi.org/10.51983/tarce-2019.8.1.2287.
[20] M.K. Neyestanaki, G. Dunca, P. Jonsson, M. Cervantes, Extending the pressure-time method to pipe with variable cross-section with 3D numerical simulations, J. Fluid Eng. (2023) 23–1247.
[21] H.W. Coleman, W.G. Steele, Experimentation, Validation, and Uncertainty Analysis for Engineers, fourth ed., 2018.

[22] S. Saemi, M.J. Cervantes, M. Raisee, A. Nourbakhsh, Numerical investigation of the pressure-time method, Flow Meas. Instrum. 55 (2017) 44–58, https://doi.org/10.1016/j.flowmeasinst.2017.05.003.
[23] F.R. Menter, Two-equation eddy-viscosity turbulence models for engineering applications, AIAA J. 32 (8) (1994) 1598–1605.
[24] ANSYS, Inc, ANSYS fluent user's guide, Release 17.2 (2016).
[25] S. SaemI, M. Raisee, M.J. Cervantes, A. Nourbakhsh, Computation of two- and three-dimensional water hammer flows, J. Hydraul. Res. 57 (2019) 386–404, https://doi.org/10.1080/00221686.2018.1459892.
[26] M.K. Neyestanaki, G. Dunca, P. Jonsson, M.J. Cervantes, A comparison of different methods for modelling water hammer valve closure with CFD, Water 15 (2023) 1510, https://doi.org/10.3390/W15081510, 1510 2023, 15.
[27] S.D. Saemi, M. Raisee, M.J. Cervantes, A. Nourbakhsh, Computation of laminar and turbulent water hammer flows, in: Proceedings of the 11th World Congress on Computational Mechanics (WCCM XI) 5th European Conference on Computational Mechanics (ECCM V) 6th European Conference on Computational Fluid Dynamics, ECFD VI, 2014.
[28] M.K. Neyestanaki, G. Dunca, P. Jonsson, M.J. Cervantes, Extending the pressure-time method to pipe with variable cross-section with three-dimensional numerical simulations, J. Fluid Eng. (2024) 146, https://doi.org/10.1115/1.4063491.
[29] M.K. Neyestanaki, G. Dunca, P. Jonsson, Numerical Investigation of the Pressure-Time Method, Head Loss in Developed and Developing Flows, Int. J. Fluid Mach. Syst. 16 (4) (2023) 332–345.

Nomenclature

A: Area [m^2]
C: The geometry factor
D: Pipe diameter [m]
$\overline{E}$: Mean error/deviation compared to the reference flow meter (%)
K: Constant coefficient of friction losses [−]
L: Pipe length [m]
N: Number of measurement
p: Average pressure at section [Pa]
p_{tap}: Measured pressure at pressure tap [Pa]
ΔP: Differential pressure [Pa]
ΔP_d: Dynamic pressure variation
ΔP_f: Pressure loss due to friction[Pa]
q: Leakage flow rate [m^3s^{-1}]
Q: Flow rate [m^3s^{-1}]
Re: Reynolds number [−]
t: Time [s]
t_f: Upper time-limit of integration of free pressure oscillation signal [s]
U: Cross-sectional velocity [ms-1]
u_i: Fluctuating velocity [m s-1]
$U_{\tau 0}$: Friction velocity at the initial steady condition [m/s]
x_i: Coordinate [m]
y^+: Dimensionless wall distance [−]

Greek Letters

α: Kinetic energy coefficient (−)
μ: Dynamic viscosity [Nsm^{-2}]
ρ: Density [kgm3]
ε: Residual
σ_r: Random uncertainty

Subscripts

c: Cross-section